# *Biodegradation, bioactivity and in vivo biocompatibility analysis of plasma electrolytic oxidized (PEO) biodegradable Mg implants*

**Mehdi Razavi [1,3,4,5 *], Mohammadhossein Fathi [1,2], Omid Savabi [3], Daryoosh Vashaee [5], Lobat Tayebi [4,6*]**

[1] Biomaterials Research Group, Department of Materials Engineering, Isfahan University of Technology, Isfahan 84156-83111, Iran
[2] Dental Materials Research Center, Isfahan University of Medical Sciences, Isfahan, Iran
[3] Torabinejad Dental Research Center, School of Dentistry, Isfahan University of Medical Sciences, Isfahan 81746-73461, Iran
[4] School of Materials Science and Engineering, Helmerich Advanced Technology Research Center, Oklahoma State University, Tulsa, OK 74106, USA
[5] School of Electrical and Computer Engineering, Helmerich Advanced Technology Research Center, Oklahoma State University, Tulsa, OK 74106, USA
[6] School of Chemical Engineering, Oklahoma State University, Stillwater, OK 74078, USA

.

## ABSTRACT

In this paper, a plasma electrolytic oxidation (PEO) coating was prepared on AZ91 magnesium (Mg) implant to improve its degradation resistance, bioactivity and biocompatibility. The phase composition and surface morphology of the samples were characterized using X-ray diffraction (XRD) and scanning electron microscope (SEM). The corrosion rate and the bioactivity behavior of the samples were investigated via electrochemical measurements and immersion tests in simulated body fluid (SBF). The biocompatibility of samples was evaluated both *in vitro* and *in vivo*. To performed *in vitro* examinations, L-929 cells were cultured on both coated and uncoated substrates, and for the *in vivo* study, samples were implanted into the greater trochanter of rabbits as our animal model. The results showed that the PEO coating enhanced the corrosion resistance and *in vitro* and *in vivo* biocompatibility of AZ91 Mg implants.

*Keywords: Plasma electrolytic Oxidation; Biodegradable Mg alloy; in vitro; ; L-929 cells; in vivo; Biomedical applications*

## 1. INTRODUCTION

Due to their strong mechanical properties, metallic implants have been widely used in bone treatment especially for large bone defects [1]. While they can help to hold bones in the proper position, metallic implants may become mobile and loose over time [2,3]. Also, they do not adjust with alterations in physiological conditions [4]. In some patients, the metal is rejected by the body or causes irritation to surrounding tissues [5]. In such cases, surgery may be required to remove the implants. However, there are potential complications from this type of surgery as the metal removal is not easy, especially with deep implants that have been in place for a long time. Moreover, removing the implant may lead to weakening of the bone where the implant was removed. To avoid such complications with metal implants,

* Corresponding authors:
*E-mail:* lobat.tayebi@okstate.edu, Tel.: +1 9185948634 (Lobat Tayebi).
*E-mail:* mehdi.razavi@okstate.edu; m.razavi@ma.iut.ac.ir , Tel.: +1 9188417078 (Mehdi Razavi).

there are enormous endeavors to replace them by biodegradable polymers [6-9]. Biodegradability of such implants is a great advantage, as they will disappear after the bone heals. However, despite the advantages, commercially, metal implants are still preferred for large bone defects. This is due to the lack of mechanical strength of many biodegradable polymers as they may not be able to bear the load of the body [6-9]. Developing a biodegradable metallic implant can incorporate all these advantages [10-12].

Mg alloys can be one of the appropriate candidates for this purpose [13-15]. Mg is an element essential to the human body and metabolism [16-19]. Mg alloys with good mechanical characteristics, such as elastic modulus and yield strength that are closer to the human bone tissue than other metallic implants, could minimize or avoid the stress shielding effect caused by stainless steel or titanium alloys [20-22]. The stiffness of Mg is about 40-45 Gpa. Although that is larger than that of the bone, which is about 20-25 Gpa, it is much lower than the stiffness of the other metallic implants such as stainless steel, cobalt alloy and titanium alloy. Thus, it may work better in avoiding the stress shielding compared to other metals [23-25]. However, Mg and its alloys are highly susceptible to corrosion in chloride-containing solutions including human body fluid or blood plasma, which has restricted their clinical applications [23,26]. To be able to use Mg alloys in medical applications, it is crucial to improve their corrosion resistance [27]. Moreover, enhancing the bioactivity and biocoampatibility of Mg alloys is also necessary to improve the healing process [28]. Surface modification of Mg alloys is a standard approach to decrease the corrosion rate and improve the bioactivity and biocompatibility [29].

Recently, plasma electrolytic oxidation (PEO) coating has become an important commercially applied protection method for some metallic alloys. During the PEO coating, a plasma is produced and an oxide layer grows. The process involves melting, flow of the melt, solidification, crystallization, partial sintering and densification of the growing oxide. PEO coatings, are more stable and can inhibit corrosion better than chemical conversion coatings [30,31]. To have the corrosion rate of Mg alloy around the bone self-healing rate, release of the hydrogen gas should be below 0.01 ml/cm$^2$/day [26]. In this case, the Mg alloy is in biomedical grade and can be used for orthopedic applications. The AZ91 Mg alloy, which we employed in this study, has around 0.01 ml/cm$^2$/day hydrogen release. We showed that the PEO coating can further decrease the corrosion rate of our Mg alloy, which can improve the degradation and enhance the bioactivity and biocompatibility to facilitate the bone treatment procedure.

In this study, the PEO coating was applied on AZ91 biodegradable Mg alloy and the preparation, corrosion resistance, in vitro bioactivity, cytocompatibility and in vivo animal study of the product are discussed.

## 2. MATERIAL AND METHODS

Plate samples (2×15×5 mm$^3$) from an AZ91 Mg ingot were prepared in our laboratory. All samples were ground with SiC emery papers of up to 600 grits, and then ultrasonically cleaned in acetone for 20 min.

The PEO coating process was conducted on a direct current (DC) power supply. The samples were used as the anode, while the stainless steel plate was the cathode. The electrolyte for PEO coating treatment was composed of sodium silicate (200 g/L) and sodium hydroxide (200 g/L). The distance between electrodes was 2 cm, time was 30 min and voltage was 60V. Coated samples were cleaned ultrasonically with acetone after the treatment and dried in air at room temperature.

The composition of the samples was characterized by X-ray diffraction (XRD, Philips X'Pert) with a Cu $k_\alpha$ radiation in the 2θ range of 10-90°. Also, X-ray diffraction was deriv ed from coated flat specimen.

The surface morphology of the samples (before and after the immersion test) was analyzed using a scanning electron microscope (Philips XL 30: Eindhoven) equipped with energy-dispersive X-ray spectroscopy (EDS).

An Ametek potentiostat (model PARSTAT 2273) was used to perform the potentiodynamic polarization and electrochemical impedance spectroscopy (EIS) tests. The samples were used as the working electrodes. The test samples were rinsed with alcohol and then with deionized water prior to the corrosion tests. A saturated calomel electrode (SCE) and platinum electrode were used as the reference electrode and counter electrode, respectively. Neutral (pH 7.4) simulated body fluid (SBF) was used as the corrosion test electrolyte. The SBF is a standard solution, which has been used to assess the biocompatibility of potential biomaterials. Thus, the behavior of samples was evaluated in the SBF to explore its possibility of being used as a biodegradable implant material. The SBF was prepared according to the procedures described by Kokubo and Takadama [32]. The polarization curves of the test samples were measured with respect to the open-circuit potential at a scan rate of 1.0 mV/s, and the EIS were measured over a frequency range from 100 kHz to 10 mHz. Before the polarization tests, the samples were kept in the solution for 1 hr to establish the open circuit potential. The corrosion parameters, including corrosion potential ($E_{corr}$), corrosion rate ($I_{corr}$), and polarization resistance ($R_p$), were obtained from the polarization and EIS curves and were used to evaluate the corrosion resistance of the test samples.

The immersion test was carried out in the SBF. The samples were immersed in the SBF in cylindrical bottles in a water bath at 37 ℃. The v olume of SBF for the immersion test was used according to the following Eq. [32]:

$$V_s = S_a/100 \quad (1)$$

where $V_s$ is the volume of SBF (l) and $S_a$ is the apparent surface area of sample ($m^2$).

The selected immersion periods were 0, 72, 168, 336, 504 and 672 hrs. After the pre-selected immersion periods, the samples were dried at room temperature. For the in vitro bioactivity evaluation, typical immersion morphology was characterized by SEM. Chromic acid was used after the immersion in SBF to remove the corrosion products [33] and the weight loss of samples was measured.

Cell culture test was performed using L-929 cell line. Dulbecco's modified Eagle's medium (DMEM, Gibco) supplemented with 10% fetal bovine serum (FBS, Gibco), and 1% penicillin streptomycin was used as the culture media. Cell viability and cell attachment examinations were performed after 2, 5 and 7 days. For MTT assay analysis, we added 400 µl MTT to each well and then replaced medium by 4 ml dimethylsulfoxide (DMSO). Cell viability was measured by absorbance of the samples as $OD_{sample}/OD_{negative\ control} * 100\%$, where $OD_{sample}$ and $OD_{negative\ control}$ are the optical density of the sample and the negative control, respectively. Cells attached on the samples were observed by SEM after fixing them on the surface by 2.5% glutaraldehyde solution.

For the in vivo animal test, rod shape samples with 6 mm length and 3 mm diameter were prepared. Rabbits with 3 kg weight were used for the surgery. The surgical procedure was conducted according to the University Ethics Committee guidelines. AZ91 and PEO samples were implanted into the greater trochanter of each rabbit. The X-ray radiography was taken

at the operation site 2 weeks after the surgery. In order to measure the changes of serum magnesium, blood samples of about 1 mL were examined from the rabbits before the implantation and at 2 weeks, 1 and 2 months of post-implantation and were analyzed using a Hitachi 911 automatic hemocyte analyzer at the clinical & anatomical pathology laboratory. The rabbits were scarified after 2 months and the new bone formation was seen by histological images under a light microscope.

## 3. RESULTS AND DISCUSSION

Fig. 1 presents the SEM morphology of the PEO coating in low (a) and high (b) magnifications, and the XRD pattern from AZ91 substrate and PEO sample (c). The surface illustrated in Fig. 1a, b showed rough areas with some pores. This structure was formed by the molten oxide and gas bubbles, which were emitted out of the plasma arc dis-charge channels. According to Fig. 1b and XRD patterns in Fig. 1c, the PEO chemical structure was mainly composed of a mixture of Mg, MgO and $Mg_2SiO_4$ due to a series of reactions at strong electrical field and in a high temperature environment during the PEO coating process. Adjustment of PEO parameters, such as the electrolyte concentrations, current density, voltage and time, strongly affects the degree of thickness, porosity and quality of the PEO layer.

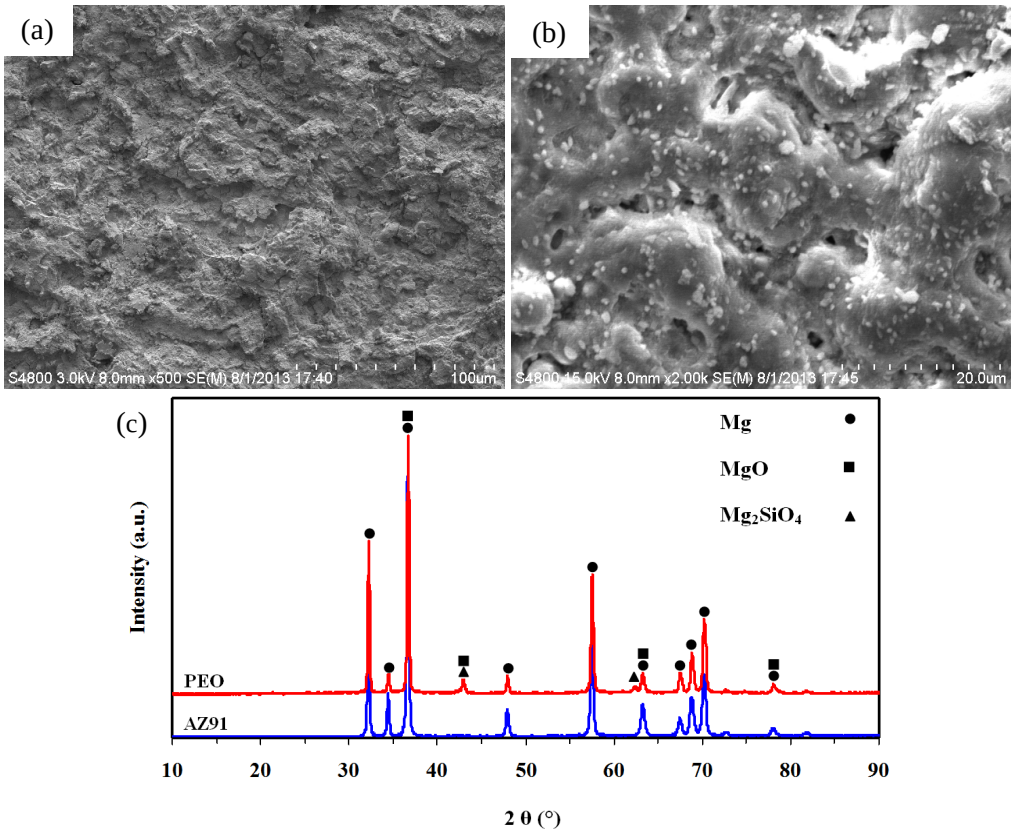


**Fig. 1. SEM morphology of the PEO coating in low (a) and high (b) magnifications, and the XRD pattern from AZ91 substrate and PEO sample (c) showing the morphology and composition of PEO coating.**

### 3.2. Electrochemical test

In order to evaluate the protection provided by PEO coating, potentiodynamic polarization experiments and electrochemical impedance spectroscopy (EIS) measurements were performed for the AZ91 and PEO coating. Fig. 2 shows the potentiodynamic polarization curves (a) and EIS plots (b) of the AZ91 and PEO coating in the SBF. The electrochemical corrosion parameters of the AZ91 and PEO coating were summarized and listed in Table 1. Generally, the cathodic polarization curve represents the cathodic hydrogen evolution while the anodic one represents the dissolution of Mg. Table 1 summarizes the corrosion potential ($E_{corr}$) and corrosion current density ($I_{corr}$) obtained by Tafel extrapolation. As seen in Table 1, it was found that the corrosion potential of the PEO coating is elevated slightly, while the corrosion current density is reduced significantly, as compared to the AZ91 samples. As shown in Table 1, regarding $E_{corr}$ (vs. SCE) values we have PEO coating (-1.56 V) > AZ91 (-1.6V) while about $I_{corr}$ values: PEO coating (53700 nA/cm$^2$) < AZ91 (63100 nA/cm$^2$). Therefore, the $E_{corr}$ value of the PEO coating is less negative than that of the AZ91 sample and the $I_{corr}$ value for the PEO coating is much lower as compared to the AZ91 sample, indicating that the PEO coating is less susceptible to corrosion.

EIS spectra further confirm the above point. According to the EIS plots, noticeable change can be found due to the presence of the PEO coating. The capacitance loop diameters of the PEO coating were larger than that of the AZ91 sample. In addition, the AZ91 sample shows a much lower Zre value compared to the PEO coating. For simplicity and for the sake of comparison, one might approximately take the real impedance at which the imaginary part vanishes for the capacitive part to be the polarization resistance $R_p$, and regard it as a measure of corrosion resistance [33]. In the high frequency region, the impedance is independent of the frequency, which is the resistance of the electrolyte between the sample and the reference electrode. At the low frequency limit, the impedance is attributed to the polarization resistance of the sample in the electrolyte. According to EIS data from Nyquist plots regarding $R_p$ values (Table 1), we have PEO coating (957.2 ohm) > AZ91 (305.5 ohm). Based on the principle of corrosion electrochemistry, the low corrosion current density, high corrosion potential, and high polarization resistance are proportional to good corrosion resistance [34]. Since the corrosion of biodegradable Mg alloys is highly problematic in biomedical applications [23], surface modifications are necessary to enhance the corrosion resistance of these alloys in biological environments. The corrosion test results of this study indicate that the corrosion resistance of AZ91 biodegradable Mg alloys was significantly increased by employing surface coating prepared by PEO method. In parallel with the electrochemical experiments, the immersion test can provide additional information regarding the corrosion resistance of the AZ91 and PEO coating for longer periods of time.

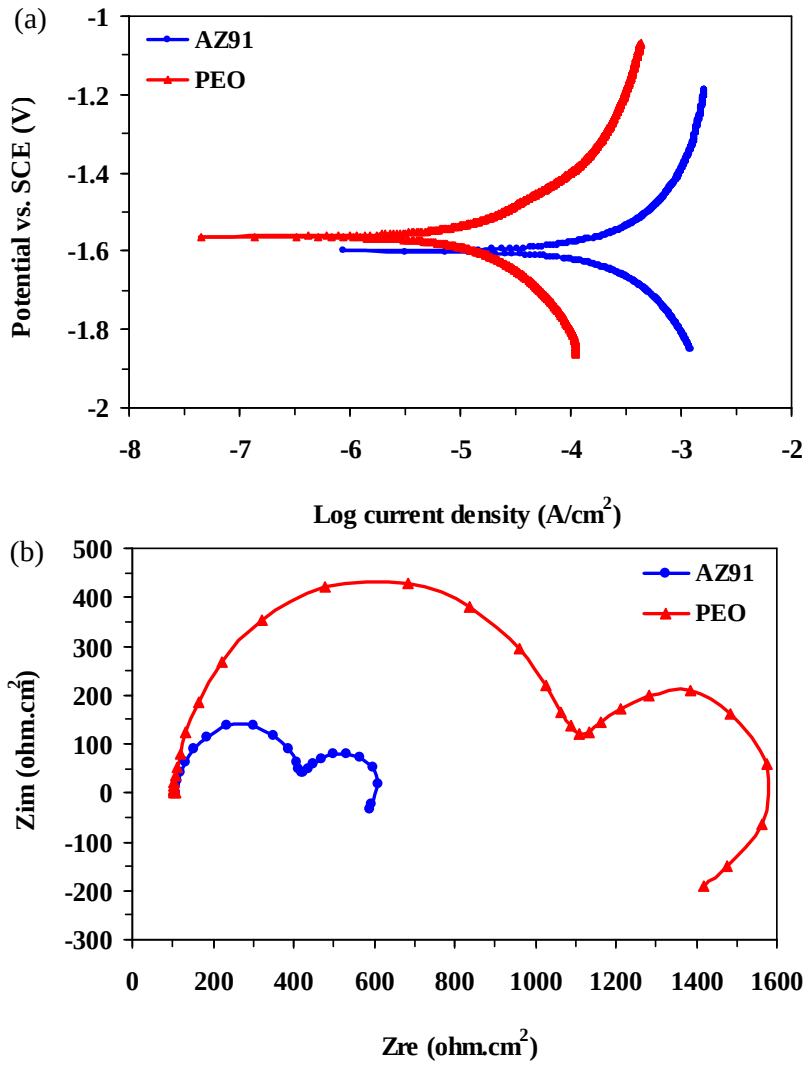


**Fig. 2. Polarization (a) and EIS (b) electrochemical tests for the AZ91 and PEO coating in the SBF showing the corrosion properties of uncoated and coated samples.**

**Table 1. Electrochemical corrosion parameters of the AZ91 and PEO coating derived from potentiodynamic polarization experiments and EIS measurements.**

| Samples | $I_{corr}$ (nA/cm$^2$) | $E_{corr}$ ($V_{SCE}$) | $R_p$ (ohm) |
|---|---|---|---|
| **AZ91** | 63100 | -1.6 | 305.5 |
| **PEO** | 53700 | -1.56 | 957.2 |

### 3.3. Immersion test

Immersion test was performed to observe the in vitro bioactivity and corrosion behavior of the samples for investigating the protective effect of the coating in long periods of time. Fig. 3 shows SEM morphology of the AZ91 (a), and PEO coating in low (b) and high (c) magnifications after 672 hrs immersion in the SBF and EDS analysis of precipitated particles in broccoli-like structure on the surface of PEO coating after 672 hrs immersion in the SBF (d). As can be seen in Fig. 3a, various areas of the AZ91 sample surface were damaged and many large and deep network-like cracks were left on the surface due to the corrosion. Several particles were also deposited on the AZ91 surface. It can be seen from Fig. 3b that the PEO coating surface morphology has been destructed and some pits and cracks appeared on the surface of the substrate. This indicates that the PEO coating has corroded during the immersion process. Moreover, particles were also deposited on the PEO coating. As can be seen in Fig. 3c, the SEM observations further indicate the broccoli-like structures on the surfaces of the PEO coating after 672 hrs immersion in the SBF solution. Comparing the corrosion and in vitro bioactivity between the AZ91 and PEO coating in different immersion times, the cracks and pits of AZ91 sample are more evident than those of the PEO coating. On the other hand, it could be observed from SEM images that the PEO coating were subjected to milder and more uniform corrosion attack than the AZ91 sample. This indicates that the degree of corrosion damage was reduced for the PEO coating compared with the AZ91 substrates, consistent with the electrochemical measurements. Moreover, in the immersion experiments, the PEO coating induced more rapid and denser precipitation of particles compared with the AZ91 substrates. EDS analysis on a square area of precipitated particles in broccoli-like structure on the surface of PEO coating after 672 hrs immersion in the SBF, as shown in Fig. 3d, indicates that the precipitates were mainly composed of Ca, P, Mg, Si and O. Mg, Si and O elements existed in the MAO coating. However, Ca and P elements and also the broccoli-like structure can show the formation of bioactive minerals on the surface. It is known that the bioactive precipitates have a chemical composition close to the natural bone, which is an indication of good bioactivity and osteoconductivity and is beneficial to increase the chances for formation of an osteointegrated interface after implantation [35-38].

In the case of Mg alloys, due to the formation of large amounts of $H_2$, increasing the reaction rate decreases precipitation of corrosion products (bone-like apatite or bioactivity) on the substrate. By PEO coating, in vitro bioactivity was increased by decreasing the hydrogen release. Moreover, forsterite ($Mg_2SiO_4$) in PEO coating may acts as the nucleation cites for apatite precipitation which can increase the bioactivity. Mg alloy is a very active alloy. When it is immersed in the SBF, Mg dissolves and turns into $Mg^{2+}$ and releases $H_2$ [39]. At the same time, $Ca(H_2PO_4)_2$ has the potential to hydrolyze and the hydrolysis product brushite ($CaHPO_4.2H_2O$) will precipitate on the surface of the Mg alloy. During this process, $Mg^{2+}$ released from the Mg alloy could react with any negative ions in the SBF, such as $PO_4^{3-}$ to form bioactive minerals [40]. Note that the hydrogen bubbles resulting from the high corrosion of the substrate can be obstacles for the newly formed particles to attach to the AZ91 substrate [39]. Stability of the implants and favorable bone–implant interface are especially important during the period of bone remolding. However, Mg alloys degrade too fast during the bone remolding period [41], leaving gaps around the implants. Therefore, the major concerns in coating of Mg alloy implants are the bioactivity issue and how they can remain intact during bone remodeling. Our results indicated that the PEO coating has improved bioactivity and osteoconductivity, and can more effectively promote the early stage of bone growth and tissue healing.

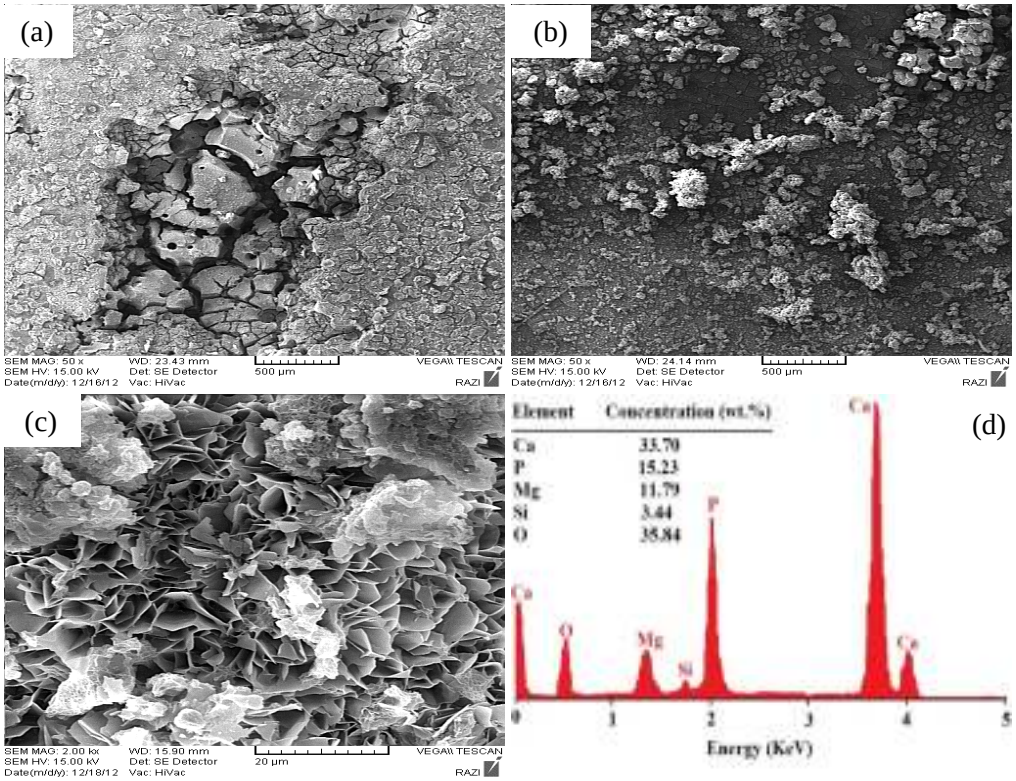


**Fig. 3. SEM morphology of the AZ91 (a), and PEO coating in low (b) and high (c) magnifications after 672 hrs immersion in the SBF and EDS analysis of precipitated particles in broccoli-like structure on the surface of PEO coating after 672 hrs immersion in the SBF (d).**

Fig. 4 shows the amount of weight loss of the AZ91 and PEO coating versus immersion time in the SBF. All samples presented a rapid increase in the weight loss at the first 72 hrs in all solutions, and then the weight loss increased gradually with the extension of immersion. In all intervals, the weight loss of AZ91 substrate was much higher than that of the PEO coating samples in the SBF solution. All samples underwent weight loss during the SBF soaking. The weight loss of the AZ91 samples resulted from the corrosion reaction of Mg while the weight loss of the PEO coating was attributed to both the dissolution of PEO coating and corrosion of the Mg substrate. The results of the immersion tests are consistent with those of the electrochemical measurements, indicating the effective protection provided by the PEO coating. Release elements during the corrosion of AZ91 include Mg, Al, Zn, and $H_2$. Mg element is biocompatible and 450 mg Mg is allowed to be released daily in the 70 Kg human body [26]. During the corrosion of AZ91, the release rate of Mg is much lower than this criterion, even in the first days of corrosion. About Al and Zn, it is in the form of $Mg_{17}Al_{12}$ and $MgZn_2$ precipitates in the Mg matrix that are biocompatible [26]. The most important element is $H_2$, which has influence on the adjacent tissues. Release of the $H_2$ gas should be below 0.01 ml/cm$^2$/day. The AZ91 Mg alloy, which we employed in this study, has below 0.01 ml/cm$^2$/day hydrogen release [26]. Overall, the AZ91 Mg alloy is biomedical grade. The release elements of PEO coating are MgO and $Mg_2SiO_4$. MgO is a biocompatible [42], and $Mg_2SiO_4$ is a bioactive and biocompatible material [43]. The corrosion proceeded according to the following reactions:

$$Mg_{(s)} + 2H_2O_{(aq)} \rightarrow Mg(OH)_{2\,(S)} + H_{2\,(g)} \quad (3)$$

$$Mg(OH)_{2\,(s)} + 2Cl^-_{(aq)} \rightarrow MgCl_{2\,(aq)} + 2OH^-_{(aq)} \quad (4)$$

Mg is a metal with a rapid corrosion rate due to its active position in the electromotive force (EMF) series. Once Mg alloys are immersed in the SBF, chemical dissolution combined with electrolyte penetration result in rapid corrosion of Mg alloys substrate. Magnesium hydroxide ($Mg(OH)_2$) on the surface of Mg alloys , from reaction (3), reacts with chloride ions in the SBF to form the soluble $MgCl_2$ as can be seen in reaction (4) [42]. Thereafter, the corrosion products layers, which mainly consist of $Mg(OH)_2$, gradually thicken and the amount of corrosion decreases by immersion time. Although $Mg(OH)_2$ forms on the surface of Mg alloys, unfortunately, this layer is too porous to effectively protect the substrate from corrosion. Thus, the system suffers from a continuous weight loss at the final stage, which leads to dissolution of the Mg alloy. Note that precipitation of corrosion products on the surface of samples immersed in the SBF solution not only improves the in vitro bioactivity but also decreases the weight loss rate, significantly [35-38].

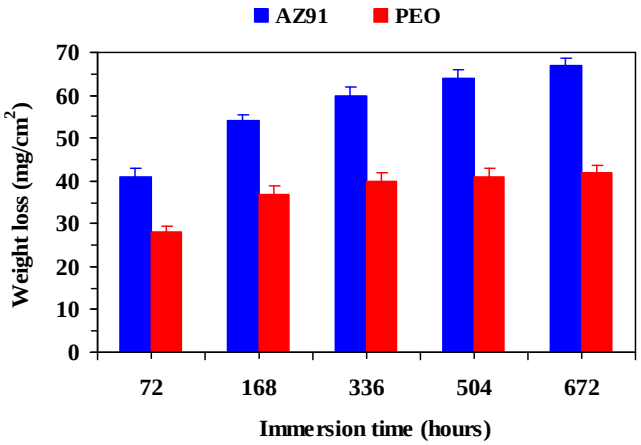


**Fig. 4. The amount of weight loss of the AZ91 and PEO coating versus immersion time in the SBF.**

### 3.4. Cell culture test

Table 2 presents the relative cell viability (% of control) of L-929 cells after 2, 5, and 7 days of incubation on the AZ91, and PEO coating. Based on the Table, the cell viability on the PEO samples is higher compared to AZ91 sample where the amount of cell viability increased from 70 % at 2 days incubation to 85 % at 7 days but for AZ91 sample, it changed from 50 % at 2 days incubation to 58 % at 7 days incubation.

**Table 2. The relative cell viability (% of control) of L-929 cells after 2, 5, and 7 days of incubation on the AZ91, and PEO coating.**

| Cell viability (%) | AZ91 | PEO |
|---|---|---|
| **2 days** | 50 ± 3 | 70 ± 5 |
| **5 days** | 55 ± 5 | 80 ± 6 |
| **7 days** | 58 ± 7 | 85 ± 7 |

Fig. 5 presents the pH value (a), and Mg ion concentration of culture medium DMEM with L-929 cells (b) after 2, 5, and 7 days of incubation on the AZ91, and PEO coating. According to Fig. 7a, the pH increase of the PEO sample is slower than that of the AZ91 sample. The pH value of the AZ91 substrate increased to 8.8 and 9.5 after 2 and 7 days culture time, respectively. However, for the PEO sample it was 8.1 and 8.8 after 2 and 7 days, respectively. According to Fig. 7b, Compared to the AZ91 sample, the PEO coated samples present a much lower release of Mg ion. After 7 days, the Mg ion concentration for the PEO and AZ91 samples was 25 and 30 ppm, respectively. It is worth mentioning that the critical concentration of Mg ion for cytotoxicity is 40-60 ppm [44], and the Mg ion released from all samples in our study is under this amount. Cell viability depends on the cultural environment. For Mg alloys, the pH value and hydrogen evolution can adversely affect the cytocompatibility. The higher pH value and rapid hydrogen evolution results in less cell attachment, and then leads to less cell viability [45]. The PEO layer acts as a passive layer between the substrate and corrosive environment and reduces the degradation of the Mg substrate. This in turn slows down the pH increase and hydrogen evolution rate of the Mg sample. Hence, it creates a relatively stable interface for the cell adhesion and growth resulting in enhanced cytocompatibility.

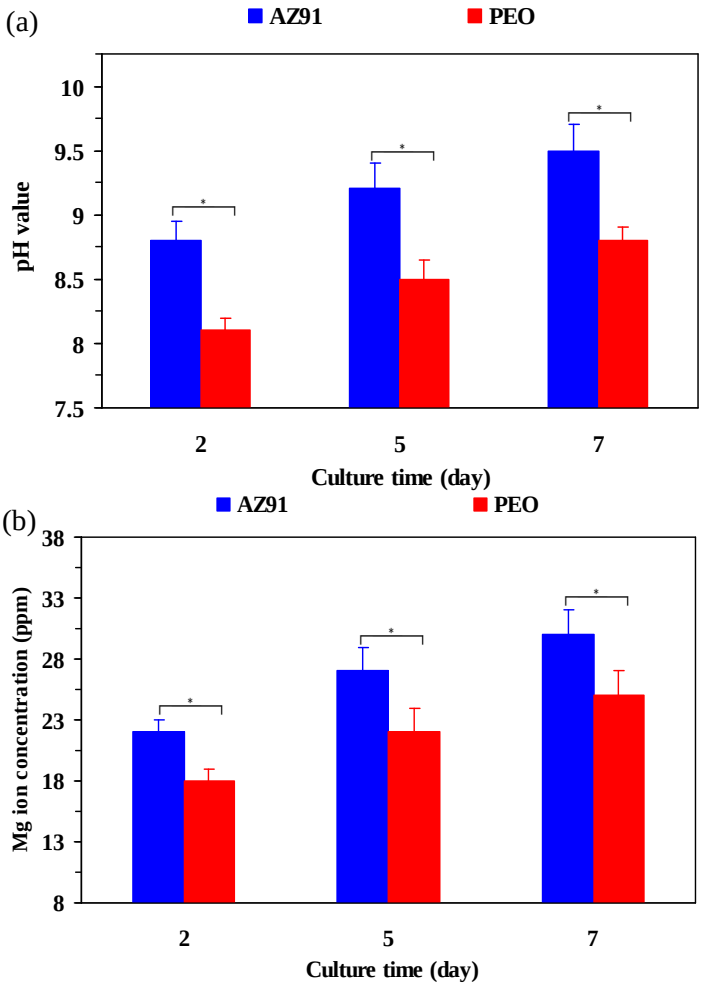


**Fig. 5. pH value (a), and Mg ion concentration of culture medium DMEM with L-929 cells (b) after 2, 5, and 7 days of incubation on the AZ91, and PEO coating.**

### 3.5. In vivo animal test

Fig. 6 shows the surgery images during the implantation of AZ91 (a) and PEO (b) implants, X-ray radiography images from AZ91 (c) and PEO (d) implants after 2 months implantation, and histological analysis of the bone surrounding AZ91 (e) and PEO (f) coated implants after 2 months post-operation. According to the X-ray radiography images, gas formation can be observed around the both implanted samples. However, the AZ91 sample shows more gas bubbles compared to the PEO sample due to its faster corrosion rate. According to the histological images, in comparing the amount of new bone formation, it was found that the uncoated AZ91 sample had the less amount of new bone formation than the PEO coated samples. Moreover, the amount of inflammation around the AZ91 implant was more than PEO implants. Also, new bone volume for the PEO coated implants are more compact and uniform than the AZ91 implants indicating that the coated Mg alloy implant is more compatible for bone growth at the early healing process. higher amount of bone formation and better quality around the PEO coated samples compared to the uncoated AZ91 samples can mainly due to the lower degradation rate which leads to slower hydrogen release, as formation of hydrogen bubbles disturb the bone reaction and callus production, resulting in less new bone formation [46,47].

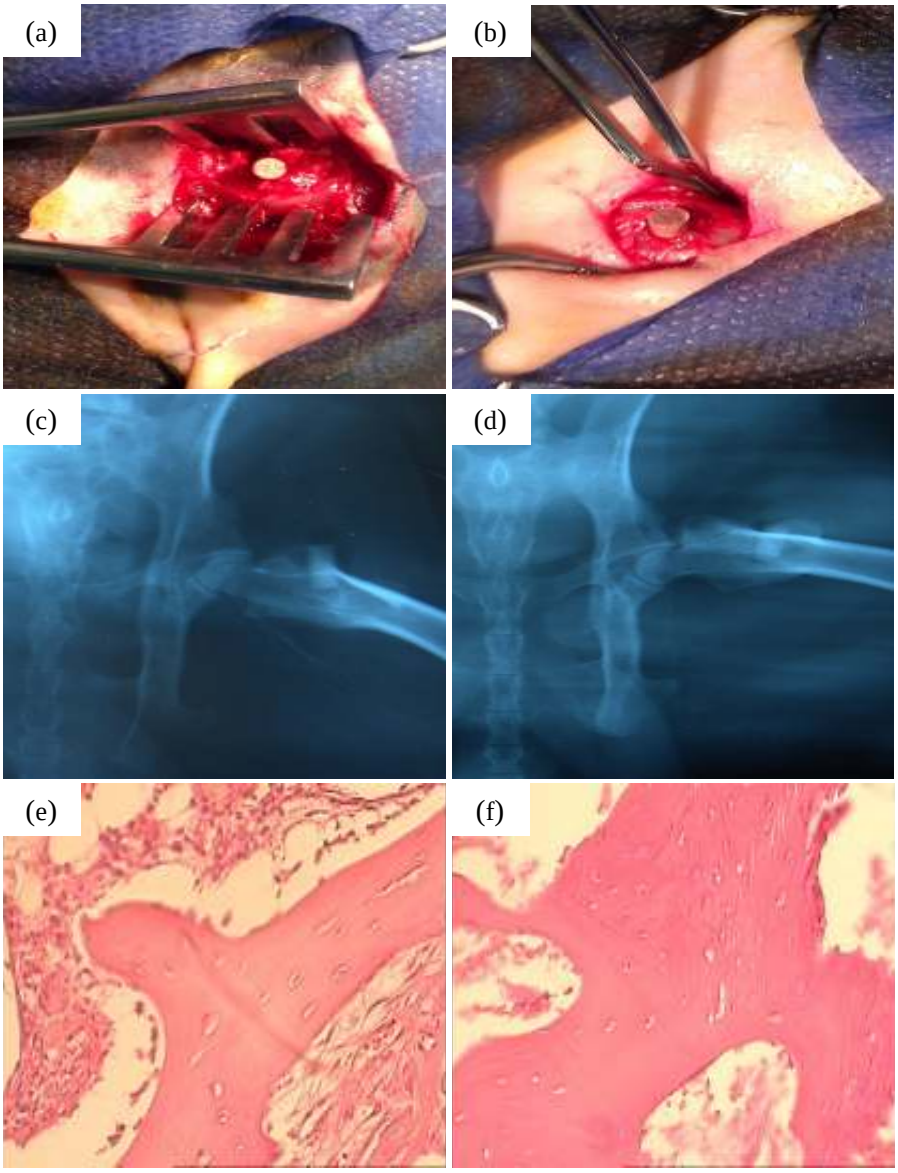


**Fig. 6. Surgery images during the implantation of AZ91 (a) and PEO (b) implants, X-ray radiography images from AZ91 (c) and PEO (d) implants after 2 months implantation, and histological analysis of the bone surrounding AZ91 (e) and PEO (f) implants after 2 months post-operation.**

The serum magnesium in blood for AZ91 and PEO implants versus post-operation time is presented in Fig. 7. The serum magnesium of all rabbits at the time point 0 was the same, and after the implantation this value increased for all samples. The normal range of serum magnesium level is 20 ppm [48], and for all samples in our study, this value is below 20 ppm. Compared to the uncoated AZ91 samples, the amount was less in magnesium ions for the PEO coated implant before and after implantation, indicating that the in vivo biodegradation of the PEO coated implant did not induce a great increase of Mg ions.

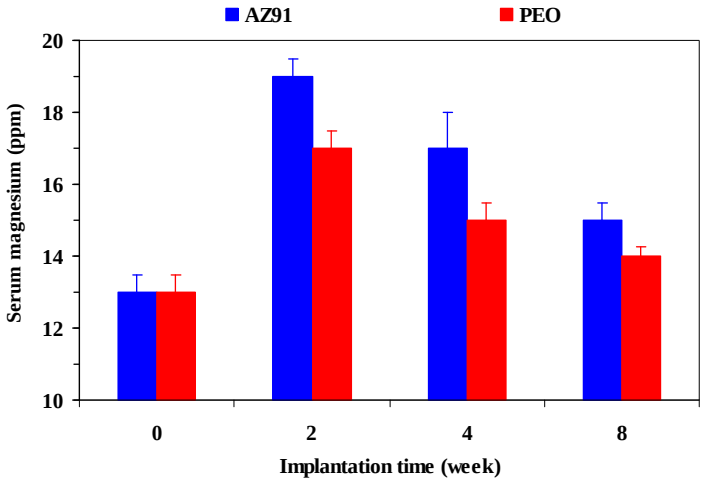


**Fig. 7. The serum magnesium in blood for AZ91 and PEO implants versus post-operation time.**

The weight loss of implanted samples after 2 months post operation was measured and presented in Table 3. The weight loss of the PEO and AZ91 samples were 16, and 25 mg/cm$^2$, respectively, which indicates the PEO implant has improved degradation resistance compared to the AZ91 sample.

**Table 3. The amount of weight loss for the AZ91, and PEO coated samples after 2 months implantation.**

| sample | AZ91 | PEO |
|---|---|---|
| Weight loss (mg/cm$^2$) | 25 | 16 |

## 4. CONCLUSION

The corrosion resistance, in vitro bioactivity and biocompatibility of biodegradable Mg alloy was increased by the Plasma electrolytic oxidation method.

## ACKNOWLEDGEMENTS

The authors are thankful for the contributions of Isfahan University of Technology, Torabinejad Dental Research Center, Oklahoma Center for Advancement of Science and Technology (Grant no. AR131-054 8161), AFOSR (Grant no. FA9550-10-1-0010) and the National Science Foundation (NSF, Grant no. 0933763).

## COMPETING INTERESTS

Authors have declared that no competing interests exist.

## ETHICAL APPROVAL (WHERE EVER APPLICABLE)

All authors hereby declare that "Principles of laboratory animal care" were followed, as well as specific national laws where applicable. All experiments have been examined and approved by the appropriate ethics committee.

## REFERENCES


[1] Matsuno H, Yokoyama A, Watari F, Uo M, Kawasaki T. Biocompatibility and osteogenesis of refractory metal implants, titanium, hafnium, niobium, tantalum and rhenium. Biomaterials 2001;22:1253–1262.

[2] Huiskes R, Weinans H, Vanrietbergen B. The relationship between stress shielding and bone resorption around total hip stems and the effects of flexible materials. Clin Orthop Relat R 1992;274:124–134.

[3] Webster TJ, Siegel RW, Bizios R. Design and evaluation of nanophase alumina for orthopaedic/dental applications. Nanostruct Mater 1999;12:983–986.

[4] Piehler HR. Future of medicine. Biomaterials 2000;25:67–70.

[5] Krecisz B, Kiec-swierczynska M, Bakowicz-mitura K. Allergy to metals as a cause of orthopedic implant failure. Int J Occup Med Environ Health 2006;19:178–180.

[6] Nejati E, Mirzadeh H, Zandi M. Synthesis and characterization of nano–hydroxyapatite rods/poly(L-lactide acid) composite scaffolds for bone tissue engineering. Comp Part A 2008;39:1589–1596.

[7] Lee SJ, Lim GJ, Lee J, Atala A, Yoo JJ. In vitro evaluation of a poly(lactide-co-glycolide)–collagen composite scaffold for bone regeneration. Biomaterials 2006;27:3466–3472.

[8] Fei ZQ, Hu Y, Wu, Wu H, Lu R, Bai J, Song H. Preparation and property of a novel bone graft composite consisting of rhBMP–2 loaded PLGA microspheres and calcium phosphate cement. J Mater Sci: Mater Med. 2008;19:1109–1116.

[9] Zhao J, Guo LY, Yang XB, Weng J. Preparation of bioactive porous HA/PCL composite scaffolds. App. Surf. Sci. 2001;255:2942–2946.

[10] Fathi MH, Meratian M, Razavi M. Novel Magnesium-nano Fluorapatite Metal Matrix Nanocomposite with Improved Biodegradation Behavior. J Biomed Nanotechnol 2011;7:1-5.

[11] Razavi M, Fathi MH, Savabi O, Boroni M. A Review of Degradation Properties of Mg Based Biodegradable Implants. Research and Reviews in Materials Science and Chemistry 2012;1:15-58.

[12] Razavi M, Fathi MH, Savabi O, Razavi SM, Hashemi Beni B, Vashaee D, Tayebi L. Controlling the degradation rate of bioactive magnesium implants by electrophoretic deposition of akermanite coating. Ceram Int 2014;40:3865–3872.

[13] Witte F, Kaese V, Haferkamp H, Switzer E, Meyer–Lindenberg A, Wirth CJ, Windhagen H. In vivo corrosion of four magnesium alloys and the associated bone respone. Biomaterials 2005;26:3557–3563.

[14] Witte F, Fischer J, Nellesen J, Crostack HA, Kaese V, Pisch A, Beckmanne F, Windhagen H: In vitro and in vivo corrosion measurement of magnesium alloys. Biomaterials 2006;27:1013–1018.

[15] Xu LP, Yu GN, Zhang EL, Pan F, Yang K. In vivo corrosion behavior of Mg–Mn–Zn alloy for bone implant application. J Biomed Mater Res 2007;83:703–711.

[16] Klaue K, Fengels I, Perren SM. Long-term effects of plate osteosynthesis: comparison of four different plates. Injury 2000;31:51–62.

[17] Wolf FI, Cittadini A. Chemistry and biochemistry of magnesium. Mol Aspects Med 2003;24:3–9.

[18] Rude RK. Magnesium Deficiency: A Cause of Heterogenous Disease in Humans. J Bone Miner Res 1998;13:49–58.

[19] Rude RK, Gruber HE. Magnesium deficiency and osteoporosis: Animal and human observations. J Nutr Biochem 2004;15:710–716.

[20] Razavi M, Fathi MH, Savabi O, Razavi SM, Hashemi Beni B, Vashaee D, Tayebi L. Surface modification of magnesium alloy implants by nanostructured bredigite coating. Mater Lett 2013;113:174–178.

[21] Razavi M, Fathi MH, Savabi O, Razavi SM, Hashemi Beni B, Vashaee D, Tayebi L. Coating of biodegradable magnesium alloy bone implants usingnanostructured diopside (CaMgSi2O6). Appl Surf Sci 2014; 288:130– 137.

[22] Razavi M, Fathi MH, Savabi O, Hashemi Beni B, Vashaee D, Tayebi L. Surface microstructure and in vitro analysis of nanostructured akermanite ($Ca_2MgSi_2O_7$) coating on biodegradable magnesium alloy for biomedical applications, Coll Surf B: Biointerf doi:10.1016/j.colsurfb.2013.12.011.

[23] Staiger MP, Pietak AM, Huadmai J, Dias G. Magnesium and its alloys as orthopedic biomaterials: a review. Biomaterials 2006;27:1728–1734.

[24] Saris NE, Mervaala E, Karppanen H, Khawaja JA, Lewenstam A. Magnesium: an update on physiological, clinical, and analytical aspects. Clin Chim Acta 2000;294,1–26.

[25] Nagels J, Stokdijk M, Rozing PM. Stress shielding and bone resorption in shoulder arthroplasty. J Shoulder Elbow Surg 2003;12:35–39.

[26] Song G. Control of biodegradation of biocompatible magnesium alloys. Corros Sci 2007;49:1696–1701.

[27] Razavi M, Fathi MH, Savabi O, Razavi SM, Hashemi Beni B, Vashaee D, Tayebi L. Nanostructured merwinite bioceramic coating on Mg alloy deposited by electrophoretic deposition, Ceram Int, doi: 10.1016/j.ceramint.2014.02.020.

[28] Song YW, Shan DY, Han EH. Electrodeposition of hydroxyapatite coatinging on AZ91D magnesium alloy for biomaterial application. Mater Lett 2008;62:3276–3279.

[29] Razavi M, Fathi MH, Meratian M. Microstructure, mechanical properties and bio–corrosion evaluation of biodegradable AZ91–FA nanocomposites for biomedical applications. Mater Sci Eng A 2010;527:6938–6944.

[30] Razavi M, Fathi MH, Meratian M. Bio-corrosion behavior of magnesium–fluorapatite nanocomposite for biomedical applications. Mater Lett 2010;64:2487–2490.

[31] Razavi M, Fathi MH, Meratian M. Fabrication and characterization of magnesium–fluorapatite nanocomposite for biomedical applications. Mater Charact 2010;61:1363–1370.

[32] Kokubo T, Takadama H. How useful is SBF in predicting in vivo bone bioactivity?.Biomaterials 2006;27:2907–2915.

[33] Blawert C, Dietzel W, Ghali E, Song G. Anodizing treatments for magnesium alloys and their effect on corrosion resistance in various environments. Adv Eng Mater 2006;8:511–533.

[34] Chiu KY, Wong MH, Cheng FT, Man HC. Characterization and corrosion studies of fluoride conversion coating on degradable Mg implants. Surf Coat Technol 2007;202:590–598.

[35] Cui X, Li Y, Li Q, Jin G, Ding M, Wang F. Influence of phytic acid concentration on performance of phytic acid conversion coatings on the AZ91D magnesium alloy. Mater Chemist Phys 2008;111:503–507.

[36] Lee KY, Park M, Kim HM, Lim YJ, Chun HJ, Kim H, Moon SH. Ceramic bioactivity: progresses, challenges and perspectives. Biomed Mater 2006;1:31–37.

[37] Li PJ, Kangasniemi I, Degroot K, Kokubo T. Bone–like hydroxyapatite induction by a gel–derived titania on a titanium substrate. J Am Ceram Soc 1994;77:1307–1312.

[38] Larsen MJ, Pearce EIF. Dissolution of powdered human enamel suspended in acid solutions at a high solid/solution ratio under a 5% $CO_2$atmosphere at 20 ℃. Arch Oral Biol 1997;42:657–663.

[39] Kouisni L, Azzi M, Zertoubi M, Dalard F, Maximovitch S. Phosphate coatings on magnesium alloy AM60 part 1: study of the formation and the growth of zinc phosphate films. Surf Coat Technol 2004;185:58–67.

[40] Feng B, Weng J, Yang BC, Qu SX, Zhang XD. Characterization of titanium surfaces with calcium and phosphate and osteoblast adhesion. Biomater. 2004;25:3421–3428.

[41] Zhang Y, Yan C, Wang F, Li W. Electrochemical behavior of anodized Mg alloy AZ91D in chloride containing aqueous solution. Corros Sci 2005;47:2816–2831.

[42] Hornberger H, Virtanen S, Boccaccini AR. Biomedical coatings on magnesium alloys – A review. Acta Biomater. 2012;8:2442–2455.

[43] Kharaziha M, Fathi MH. Synthesis and characterization of bioactive forsterite nanopowder. Ceram Int 2009;35:2449–2454.

519 [44] Zreiqat H, Howlett C, Zannettino A, Evans P, Schulze-Tanzil G, Knabe C, Shakibaei M.
520 Mechanisms of magnesium-stimulated adhesion of osteoblastic cells to commonly used
521 orthopaedic implants, Biomed Mater Res, 2002;62:175-184.

522 [45] Wong HM, Yeung KW, Lam KO, Tam V, Chu PK, Luk KD, Cheung K. A biodegradable
523 polymer-based coating to control the performance of magnesium alloy orthopaedic implants.
524 Biomaterials 2010;31:2084-2096.

525 [46] Serre C, Papillard M, Chavassieux P, Voegel J, Boivin G. Influence of magnesium
526 substitution on a collagen–apatite biomaterial on the production of a calcifying matrix by
527 human osteoblasts. J biomed Mater Res 1998 (42) 626-633.

528 [47] Witte F, Kaese V, Haferkamp H, Switzer E, Meyer-Lindenberg A, Wirth C, Windhagen
529 H. In vivo corrosion of four magnesium alloys and the associated bone response.
530 Biomaterials 26 (2005) 3557-3563.

531 [48] Rettig R, Virtanen S. Composition of corrosion layers on a magnesium rare-earth alloy
532 in simulated body fluids. J Biomed Mater Res Part A 88 (2009) 359-369.

533

534